INTERNATIONAL JOURNAL FOR NUMERICAL METHODS IN FLUIDS, VOL. 24, 579–593 (1997)

EULERIAN–LAGRANGIAN COMPUTATIONS ON PHASE DISTRIBUTION OF TWO-PHASE BUBBLY FLOWS

T. C. KUO, C. PAN AND C. C. CHIENG

Department of Nuclear Engineering, National Tsing-Hua University, 101, Sec. 2, Kuang-Fu Road, Hsinchu, Taiwan

AND

A. S. YANG

Satellite Development Division, National Space Program Office, 2F, No. 9, R&D Road 1, Science-Based Industrial Park, Hsinchu, Taiwan

SUMMARY

A comprehensively theoretical model is developed and numerically solved to investigate the phase distribution phenomena in a two-dimensional, axisymmetric, developing, two-phase bubbly flow. The Eulerian approach treats the fluid phase as a continuum and solved Eulerian conservation equations for the liquid phase. The Lagrangian bubbles are tracked by solving the equation of motion for the gas phase. The interphase momentum changes are included in the equations. The numerical model successfully predicts detailed flow velocity profiles for both liquid and gas phases. The development of the wall-peaking phenomenon of the void fraction and velocity profiles is also characterized for the developing flow. For 42 experiments in which the mean void fraction is less than 20 per cent, numerical calculations demonstrate that the predictions agree well with Liu's experimental data. © 1997 by John Wiley & Sons, Ltd.

KEY WORDS: Eulerian–Lagrange computation; bubbly flow; void fraction distribution; two-fluid model; gas–liquid flow

INTRODUCTION

In a two-phase bubbly flow, the mass, momentum and energy transfer processes involved are inherently complicated and closely linked to phase distribution profiles through the strong interaction at the gas–liquid interface. The physical mechanism can only be modelled if multidimensional phenomena are accounted for. Multidimensional analyses of two-phase flows are both interesting and challenging in terms of physical modelling and numerical methodology. Numerous mathematical models have been developed to describe the mechanics of two-phase flows, e.g. the two-fluid model is the most sophisticated and acceptable one for gas–liquid two-phase flows. It is developed using a time-averaged framework which takes account of the phase change as well as the interfacial momentum and energy transport in both axial and lateral directions. Various correlations and parameters are suggested by different authors and need to be validated for different flow and heat transfer conditions.

As far as computational methodologies are concerned, two approaches can be used to predict the detailed physical mechanisms of two-phase flows: Eulerian–Eulerian and Eulerian–Lagrangian

CCC 0271–2091/97/060579–15 $17.50

Received January 1996
Revised May 1996

approaches. In the Eulerian–Eulerian approach both phases are treated as continuous media and the two phases are coupled through phase interactions. The Eulerian–Lagrangian approach treats the fluid phase as a continuum and the second phase as discrete particles (bubbles). The interactions between phases are also considered.

Numerical simulations using the Eulerian–Eulerian-type two-phase model for liquid–gas phases have been performed in recent years. However, the large differences in density and mass between air and water make the system of governing equations very stiff and difficult to converge numerically, especially in the gas phase. Therefore not only were the calculations for the gas phase conducted with simplification by solving alternative equations in previous works, but also the predicted gas velocity distributions were either not presented or not compared with experimental data.[2–5] Those reports reveal the difficulty in predicting gas velocity profiles in a reasonably accurate manner.

The Eulerian–Lagrangian approach has been widely used for gas–solid and gas–droplet two-phase flows. Crowe[6] reviewed the numerical models for dilute gas–particle flows and categorized this approach as trajectory models. These models have been very popular in predicting particulate two-phase flows.[7] The present work extends the models to study the mixing of air bubbles and water, since no work seems to have been reported previously using this approach. Because the bubbles in a liquid flow field and the interactions among bubbles are sporadic, the Lagrangian approach can not only directly simulate the movement of the dispersed phase in two-phase flows but can also eliminate the numerical diffusion of the disperse phase. In the present work a two-fluid model formulation is employed to investigate the phase distribution mechanism in a two-phase bubbly flow. For the liquid (continuous) phase the flow field is described in Eulerian co-ordinates and subsequently obtained by solving a set of partial differential equations based on the conservation of mass and momentum as well as the interfactial transfer laws. While considering the Lagrangian viewpoint for the gas (disperse) phase, each bubble is traced and observed as it moves in space. The trajectory and velocity of a bubble can eventually be determined. During the computations the interaction between the liquid flow field and the gas bubbles is defined by the gas–liquid interfactial transfer laws. After completing the calculation procedure, velocity distributions for both liquid and gas phases, void fraction profile and liquid phase turbulent properties can be obtained simultaneously. The validity of the present model is verified by comparing the predicted results with the experimental data of Liu.[8]

PHYSICAL AND MATHEMATICAL MODEL ASSUMPTIONS

The following assumptions are made in this study to simplify the analysis.

1. The bubbles are assumed to be spherical despite the fact that they may be ellipsoidal or even ‘wobbly’ in shape.
2. The bubble size remains unchanged.
3. The number of bubbles is conserved, i.e. no bubble break-up or coalescence occurs.

MODELLING FOR LIQUID PHASE

In this study the general form of the two-fluid model proposed by Ishii[9] is employed for the liquid phase. The following equations can be obtained by applying the time-averaging operation to multidimensional conservation equations for mass and momentum.

Continuity equation

$$\frac{\partial(\alpha_L \rho_L)}{\partial t} + \nabla \cdot (\alpha_L \rho_L \bar{\mathbf{U}}_L) = 0, \tag{1}$$

where $\bar{\mathbf{U}}_t$ and α_L are the time-averaged velocity and volumetric fraction for the liquid phase respectively and ρ_L is the liquid density. This equation states that there is no net production of mass. The summation of the volumetric fractions for the liquid and gas phases is equal to unity, implying that the mixture is saturated. Thus

$$\alpha_L + \alpha_G = 1, \tag{2}$$

where the subscripts L and G refer to the liquid and gas phases respectively.

Momentum equation

$$\frac{\partial(\alpha_L \rho_L \bar{\mathbf{U}}_L)}{\partial t} + \nabla \cdot (\alpha_L \rho_L \bar{\mathbf{U}}_L \bar{\mathbf{U}}_L) - \alpha_L \nabla \bar{P} + \nabla \cdot \alpha_L T_L^t + \alpha_L \rho_L \mathbf{g} + \mathbf{M}_L, \tag{3}$$

where $\bar{P}$ is the pressure, $\mathbf{g}$ is the gravitational acceleration, $\mathbf{T}_L^t$ is the stress tensor and $\mathbf{M}_L$ is the volumetric momentum transfer rate at the liquid–gas interface, which consists of several parts as shown below:

$$\mathbf{M}_L = \mathbf{M}_L^D + \mathbf{M}_L^L + \mathbf{M}_L^W + \mathbf{M}_L^{etc.}. \tag{4}$$

The first three terms in (4), $\mathbf{M}_L^D$, $\mathbf{M}_L^L$ and $\mathbf{M}_L^W$, represent the momentum transfer at the liquid–gas interface due to interfacial drag, lift and wall forces respectively. The last term $\mathbf{M}_L^{etc.}$ includes such effects as the virtual mass, Busset force and collision forces, which are neglected in this study.

The interfacial drag force for the liquid phase per unit volume, $\mathbf{M}_L^D$, can be derived via the model proposed by Ishii and Zuber[10] as

$$\mathbf{M}_L^D = \frac{3}{4}\frac{1}{d_b} a_G \rho_L C_D |\bar{\mathbf{U}}_G - \bar{\mathbf{U}}_L| (\bar{\mathbf{U}}_G - \bar{\mathbf{U}}_L), \tag{5}$$

where d_b is the bubble diameter and the drag coefficient C_D is expressed as[11]

$$C_D = \frac{24}{Re_b}(1 + 0{\cdot}1 Re_b^{0{\cdot}75}), \tag{6}$$

with Re_b is the bubble Reynolds number given by

$$Re_b = \frac{d_b \rho_L |\bar{\mathbf{U}}_G - \bar{\mathbf{U}}_L|}{\mu_L/(1-\alpha_G)}. \tag{7}$$

The lateral lift force $\mathbf{M}_L^L$ is obtained using the model presented by Drew and Lahey.[12] Thus we have

$$\mathbf{M}_L^L = -C_L \alpha_G \rho_L (\bar{\mathbf{U}}_G - \bar{\mathbf{U}}_L) \times (\nabla \times \bar{\mathbf{U}}_L), \tag{8}$$

where the lift coefficient C_L ranges from 0·01 (for highly viscous flow) to 0·5 (for inviscid flow) for bubbly flows according to the data of Wang *et al.*[13]

The wall force term $\mathbf{M}_L^W$ takes the form developed by Antal *et al.*,[2]

$$\mathbf{M}_L^W = -\frac{\alpha_G \rho_L |\mathbf{U}_\parallel|^2}{d_b/2}\left[C_{w1} + C_{w2}\left(\frac{d_b}{2y_0}\right)\right]\mathbf{n}_w, \tag{9}$$

where y_0 is the distance between the bubble centre and the wall,

$$\mathbf{U}_{\|} = (\bar{\mathbf{U}}_G - \bar{\mathbf{U}}_L) - [\mathbf{n}_w \cdot (\bar{\mathbf{U}}_G - \bar{\mathbf{U}}_L)]\mathbf{n}_w, \tag{10}$$

$$C_{w1} = -0{\cdot}104 - 0{\cdot}06|\bar{\mathbf{U}}_G - \bar{\mathbf{U}}_L|, \tag{11}$$

$$C_{w2} = 0{\cdot}147 \tag{12}$$

and $\mathbf{n}_w$ is the unit vector normal to the wall and pointing to the centre of the channel. This model was originally developed for laminar flow conditions, it is extended to turbulent flow conditions.

The stress tensor in (3), $\mathbf{T}_L^t$, is given by

$$\mathbf{T}_L^t = -\rho_L \overline{\mathbf{u}_L' \mathbf{u}_L'} + \mu_L \nabla \bar{\mathbf{U}}_L, \tag{13}$$

where the first term on the right-hand side is the turbulent stress tensor and the second term is the viscous stress tensor. The turbulent stress tensor can be expressed as

$$-\rho_L \overline{\mathbf{u}_L' \mathbf{u}_L'} = \mu_L' \nabla \bar{\mathbf{U}}_L. \tag{14}$$

The eddy viscosity for the liquid phase, μ_L^t, is formulated by the high-Reynolds-number form of the k–ε model as below.

TURBULENCE MODEL

Turbulent pipe flow can be a so-called benchmark flow to evaluate the constants in turbulence models for single-phase flows. Martinuzzi and Pollard[14] performed a comparative study of the prediction of developing turbulent pipe flow and found that the results obtained with the low-Reynolds-number k–ε model are in better agreement with experimental data than the results obtained with other models, especially at low Reynolds numbers. The six models they employed are high- and low-Reynolds-number versions of the k–ε model and four versions of the algebraic stress model. The prediction using the high-Reynolds-number k–ε model agrees best with measurements at a Reynolds number of 10,000 and the cases in this study are in the same range. The model in this study solves the transport equations of turbulent kinetic energy k_L and its dissipation rate ε_L and is formulated as follows.

Turbulent kinetic energy equation

$$\frac{\partial \alpha_L k_L}{\partial t} + \nabla \cdot (\alpha_L \rho_L k_L \bar{\mathbf{U}}_L) = \nabla \cdot \left(\alpha_L \frac{\mu_L^t}{\sigma_k} (\nabla k_L) \right) + \alpha_L (G_L - \rho_L \varepsilon_L) + S_L^k. \tag{15}$$

Turbulent energy dissipation rate equation

$$\frac{\partial \alpha_L \varepsilon L}{\partial t} + \nabla \cdot (\alpha_L \rho_L \varepsilon_L \bar{\mathbf{U}}_L) = \nabla \cdot \left(\alpha_L \frac{\mu_L^t}{\sigma_\varepsilon} (\nabla \varepsilon_L) \right) + \alpha_L (C_{\varepsilon 1} G_L - C_{\varepsilon 2} \rho_L \varepsilon_L) \frac{\varepsilon_L}{k_L} + S_L^\varepsilon. \tag{16}$$

The effective Prandtl numbers for the turbulent kinetic energy, σ_k, and for the dissipation rate, σ_ε, and the constants in (16), $C_{\varepsilon 1}$ and $C_{\varepsilon 2}$, are listed in Table I. These numbers are given by Launder and Spalding[15] for single-phase turbulent flows. The turbulent kinetic energy production rate G_L is expressed

$$G_L = \mu_L^t (\nabla \bar{\mathbf{U}}_L : \nabla \bar{\mathbf{U}}_L), \tag{17}$$

Table I. Constants in k–ε model[15]

C_μ	σ_k	σ_ε	$C_{\varepsilon 1}$	$C_{\varepsilon 2}$
0·09	1·0	1·3	1·44	1·92

where the eddy viscosity of the liquid phase, $\mu_{\mathrm{L}}^{\mathrm{t}}$, is given by

$$\mu_{\mathrm{L}}^{\mathrm{t}} = C_\mu \rho_{\mathrm{L}} \frac{k_{\mathrm{L}}^2}{\varepsilon_{\mathrm{L}}} + C_{\mu \mathrm{b}} \rho_{\mathrm{L}} \frac{d_{\mathrm{b}}}{2} \alpha_{\mathrm{G}} |\bar{\mathbf{U}}_{\mathrm{G}} - \bar{\mathbf{U}}_{\mathrm{L}}|. \tag{18}$$

The first term on the right-hand side of (18) is the turbulent viscosity induced by shear. As indicated in Table I, the proportionality constant C_μ for single-phase flows[15] is adopted. The second term includes the modifications due to the coexistence of liquid phase and bubbles. The formulation of the turbulence model for bubbly flow needs to be further validated. The second term accounts for the turbulence resulting from bubble agitation.[16] $C_{\mu \mathrm{b}}$ is chosen as 1·2.[16] The sources for turbulent kinetic energy and energy dissipation rate due to interfacial interaction, S_{L}^k and $S_{\mathrm{L}}^\varepsilon$ are treated using the model proposed by de Bertodano *et al.*[17]

$$S_{\mathrm{L}}^k = \mathbf{M}_{\mathrm{L}}^{\mathrm{D}} \cdot (\bar{\mathbf{U}}_{\mathrm{G}} - \bar{\mathbf{U}}_{\mathrm{L}}), \tag{19}$$

$$S_{\mathrm{L}}^\varepsilon = C_{\varepsilon 2} \frac{\varepsilon_{\mathrm{L}}}{k_{\mathrm{L}}} S_{\mathrm{L}}^k. \tag{20}$$

MODELLING FOR GAS PHASE

For the gas phase the Lagrangian (instead of the Eulerian) approach is adopted here. Bubbles are considered to be spherical particles. The changes in the shape and size of bubbles are assumed to be negligible when the bubbles pass through the flow field. There are a number of forms for the equation of motion of a small particle in a flow field and these equations are based on the equations developed by Basset, Boussinesq and Oseen. Tschen[18] extended the solution to unsteady Stokes flow in a uniform fluid and to non-uniform flows. No disturbance was unsteady Stokes flow in a uniform fluid and to non-uniform flows. No disturbance was assumed due to the existence of the particle and no particle–particle interactions were considered in the modified Tchen equation. In bubbly flow the bubble size is not negligible compared with the pipe diameter and the bubble density is very low compared with that of water, so the dominating forces of the bubble motion are the buoyancy force ($\mathbf{F}_{\mathrm{B}}$), interfacial drag ($\mathbf{F}_{\mathrm{D}}$), lift force ($\mathbf{F}_{\mathrm{I}}$) and wall force ($\mathbf{F}_{\mathrm{W}}$). Hence the following equation of motion for the bubble is employed:

$$m_{\mathrm{b}} \frac{\mathrm{d}\bar{\mathbf{U}}_{\mathrm{G}}}{\mathrm{d}t} = \mathbf{F}_{\mathrm{B}} + \mathbf{F}_{\mathrm{D}} + \mathbf{F}_{\mathrm{L}} + \mathbf{F}_{\mathrm{W}}, \tag{21}$$

where $m_{\mathrm{b}} = \rho_{\mathrm{G}} V_{\mathrm{b}}$ (V_{b} is the volume of a bubble with diameter d_{b}). The buoyancy force is

$$\mathbf{F}_{\mathrm{B}} = -(\rho_{\mathrm{L}} - \rho_{\mathrm{G}}) V_{\mathrm{b}} \mathbf{g}. \tag{22}$$

The interfacial forces on the right-hand side of (21) can be obtained from (5), (8) and (9) using the relationship

$$\mathbf{F}_x = \mathbf{M}_{\mathrm{G}}^x V_{\mathrm{b}} / \alpha_{\mathrm{G}} \tag{23}$$

and noting that $\mathbf{M}_{\mathrm{G}}^x = -\mathbf{M}_{\mathrm{L}}^x$, where x refers to the drag force (D), lift force (L) or wall force (W).

BOUNDARY CONDITIONS

The liquid and gas phase velocities and void fraction distributions at the pipe inlet are given by experimental conditions and in this study are all uniform at the entrance of the pipe. However, the void profile is not strictly uniform at the inlet, even though bubbles are uniformly injected into the pipe. Since the bubble size is fixed and spherical in this study, the bubble radius is the minimum distance between the bubble centre point and the pipe wall. Excluding the near-wall region, the void profile in the radial direction is uniform. Given J_L, the superficial velocity of the liquid phase, J_G, the superficial velocity of the gas phase, and $\langle\alpha_G\rangle$, the mean void fraction, the liquid and gas inlet velocities can be determined as $J_L/(1-\langle\alpha_G\rangle)$ and $J_G/\langle\alpha_G\rangle$ respectively.

At the pipe wall a logarithmic velocity profile is applied to the liquid phase flow field. The wall function for turbulent kinetic energy and dissipation rate at the edge of the buffer region (where $y^+ \approx 30$) can be derived by setting the turbulent kinetic energy production rate equal to the dissipation rate. Thus

$$k_{L,p} = \left[\frac{u_\tau \kappa y}{C_\mu}\left(\frac{u_\tau^3}{\kappa y} + \frac{S_L^k}{\rho_L(1-\alpha_G)}\right)\right]^{1/2}, \tag{24}$$

$$\varepsilon_{L,p} = \frac{u_\tau^3}{\kappa y} + \frac{S_L^k}{\rho_L(1-\alpha_G)}, \tag{25}$$

where u_τ is the frictional velocity, κ is the von Karman constant and y is the distance away from the pipe wall. Along the centreline of the pipe a symmetry condition is imposed on all flow properties.

NUMERICAL METHOD AND SOLUTION PROCEDURE

The solution procedure of the present study combines the Eulerian approach for the liquid phase (continuous phase) and the Lagrangian approach for the gas phase (disperse phase) and takes the interactions between the two phases into account simultaneously. Therefore the numerical procedure in the present work can be separated into two major parts and iterations are proceeded between them until convergence is reached.

In the first part the liquid phase will be treated. The solution procedure for the liquid phase is based on the same ideas as for single-phase flow, although the additional variables of gas void fraction distribution and gas velocities need to be implemented from the initial guesses for the first iteration step or from the solution of the equation of motion for the bubbles after the mth iteration. The location of the void fraction in the staggered grid is at the same nodes as the pressure. The conservation equations (1) and (3) of mass and momentum are discretized by a control volume approach with a 49×21 staggered grid system. The SIMPLEC scheme[19] is adopted for the velocity–pressure coupling. The liquid phase velocities in both axial and radial directions, the turbulent kinetic energy, turbulent kinetic energy dissipation rate and system pressure can be obtained until convergent criteria are satisfied.

In the second part the gas phase velocity field is obtained by injecting N bubbles at the inlet of the vertical pipe. The injected bubbles are uniformly distributed at the inlet. The equation of motion for N bubbles, equation (21), is solved over time intervals Δt ranging from $6{\cdot}75 \times 10^{-5}$ to $2{\cdot}85 \times 10^{-4}$ s, which are about two orders less than the time scale of turbulent eddies. The use of these smaller time intervals will ensure that the bubble influence on the fluid is under control and that convergence can be reached during the time interval. The ith bubble location at time $t+\Delta t$, $\mathbf{x}_{t+\Delta t}^i$, is determined by

$$\mathbf{x}_{t+\Delta t}^i = \mathbf{x}_t^i + \mathbf{V}_G^i \times \Delta t, \tag{26}$$

where $\mathbf{x}_t^i$ is the location of the injected bubbles at the beginning of the time interval between t and $t + \Delta t$. Therefore every bubble is tracked and recorded while travelling in the liquid flow. Based on the known information on bubble size and tracks, the updated void fraction distribution can be obtained by summing the volumes of all sampled bubbles which appear in the control volume of each computational node and then normalizing the sum by the mean void fraction. Meanwhile, updated gas velocities U_G and V_G at the specific computational cell are obtained by averaging the velocities of those bubbles passing the specific computational cell. To examine the sensitivity of the number of bubbles injected to the void fraction profile, numerical experiments using different numbers (N) of bubbles have been conducted. Those results indicate that the void fractions predicted by 1000 bubbles differ from those for 2000 bubbles by a maximum value of 0·1% of the void fraction at each node.

The detailed procedure of the entire computation is as follows.

1. Guess the initial void fraction distribution, velocity profiles of both phases and pressure as follows: $\alpha = \alpha_0$; $U_{L,0}$ (liquid inlet velocity) = const.; $U_{G,0}$ (gas inlet velocity) = const.; $V_{L,0} = V_{G,0} = 0$; $P_0 = \rho_L g(L_{pipe} - x)$.
2. Solve the flow field of the liquid phase with the first guess of step 1; thus $U_{L,1}$, $V_{L,1}$ and P_1 are obtained with α_0, $U_{G,0}$ and $V_{G,0}$.
3. Inject 1000 bubbles at the inlet uniformly and trace the bubble movements and tracks until they leave the outlet of the pipe. It usually takes 3000–5000 time steps for these bubbles to pass through the channel. Collecting the bubble velocities and tracks at each computational cell will determine the updated void fraction α_1 and gas velocities $U_{G,1}$ and $V_{G,1}$.
4. Obtain the updated liquid phase velocities $U_{L,2}$, $V_{L,2}$ and pressure P_2 by repeating step 2 with α_1, $U_{G,1}$ and $V_{G,1}$.
5. Repeat step 3 to find α_2, $U_{G,2}$ and $V_{G,2}$; this is the second iteration.
6. Repeat the iteration loop of steps 2–5 until the convergence criterion

$$\left|\frac{\alpha_m - \alpha_{m+1}}{\alpha_m}\right| \leqslant 0{\cdot}1\%$$

is reached, i.e. compare the void fractions of the mth and $(m+1)$th iterations. This usually takes 30–40 iterations in the present work.

TEST GEOMETRY AND CONDITIONS

A two-dimensional, axisymmetric analysis is performed next. Since a comparison is made of the numerical calculations with the data reported by Liu,[8] the experimental conditions listed in Reference 8 are employed in the present analyses. The pipe diameter D is 38·1 mm. Though the length of the test section in Liu's work is 2·8 m, the calculational domain only extends to 2·286 m ($\sim 60D$) in this study, since no experimental data are presented for $L/D > 36{\cdot}0$ in Reference 8. The calculated results are compared with the experimental data at $L/D = 36{\cdot}0$ for all cases. Moreover, four more inputs are required for each simulation: the superficial velocities for the liquid and gas phases, mean void fraction and mean bubble diameter. The superficial velocities for the liquid phase are 0·376, 0·535, 0·753, 0·973, 1·087 and 1·391 m s^{-1}, while the superficial velocities for the gas phase are 0·027, 0·067, 0·112, 0·180, 0·230, 0·293 and 0·347 m s^{-1}. The mean void fraction and mean bubble diameter range 1·48% to 41·68% and from 2·0 to 4·2 mm respectively. A total of 42 sets of experiments in Liu's work have been simulated.

RESULTS AND DISCUSSIONS

One of the 42 experiments has been chosen to perform a grid dependence test for the numerical simulation. The liquid and gas superficial velocities are 1·087 and 0·112 m s^{-1} respectively. The mean void fraction for this case is 7·37%. The fine and coarse grid systems consist of 49 × 33 and 49 × 21 grid points respectively. The y^+-values for the nodes next to the pipe wall are about 35 for both grid systems. Insignificant differences in the velocities and void fraction are obtained using these two grids. Thus the 49 × 21 grid system is employed to perform all computations.

Figure 1 shows typical calculated results of the development of the liquid velocity field, gas velocity field and some bubble tracks. It demonstrates that the boundary layer thickness decreases for the liquid phase and the gas velocity increases near the pipe centreline as the flow goes downstream (i.e. L/D increases). A tendency arises in which bubbles move towards the pipe wall to some extent as they go downstream. The radial component of the gas velocity vector does not vanish even near the exit of the pipe, which implies that the flow is not fully developed yet. For the present investigation, bubbles are injected uniformly into the pipe. The tracks shown in Figure 1(c) illustrate the mean bubble migration behaviour, while a single bubble actually moves in a zigzag path in the experiments.

Figure 2 provides a detailed description of the velocity profile development for both liquid and gas phases. Figures 1 and 2 indicate that the axial velocity profiles for both liquid and gas phases do not change significantly for $L/D > 20{\cdot}0$ and the so-called fully developed velocity profile is never actually reached in a strict sense, especially for the gas phase. A direct comparison is also made of the model predictions with Liu's[8] data. Data set I of Liu[8] was obtained by a hot film boundary layer probe for liquid velocity and a dual-sensor electrical resistivity probe for gas velocity. Additionally,

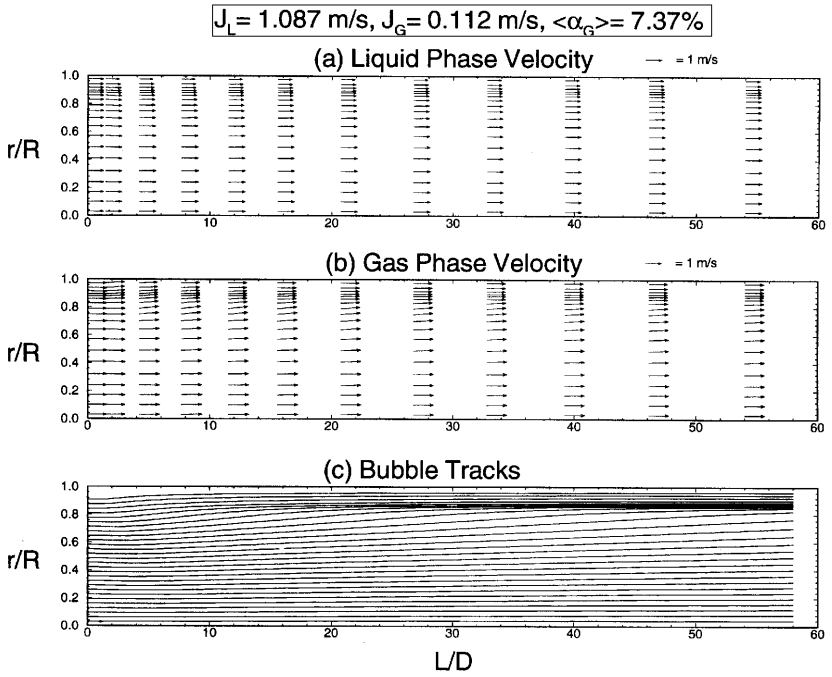

Figure 1. Development of (a) liquid velocity field, (b) gas velocity field and (c) some tracks traced by bubbles injected into liquid flow field. The superficial velocities for the liquid and gas phases are 1·087 and 0·112 m s^{-1} respectively

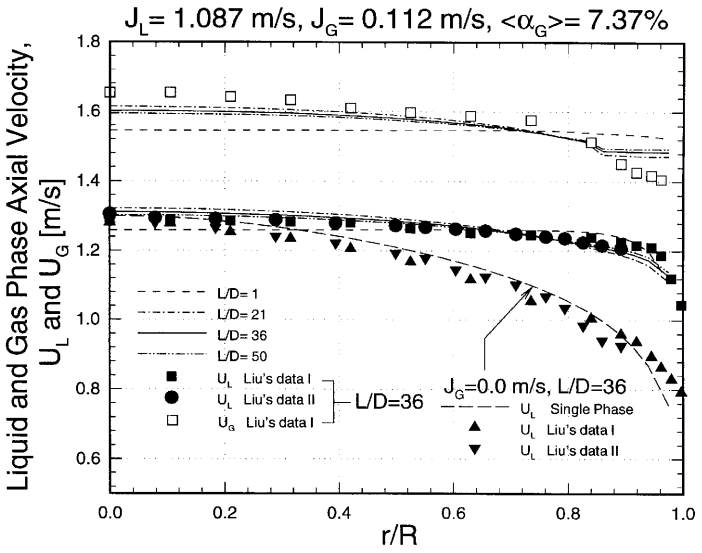

Figure 2. Development of liquid and gas velocity distributions

data set II is obtained by a dual-sensor X-type hot film probe. For both single-phase and two-phase conditions the predictions correlate well with the experimental data, thereby confirming the validity of the present model. The single-phase velocity profile prediction is satisfactory when the calculated profiles are compared with the measurements. However, the measured velocity is slightly higher than the predicted value near the wall. The difficulties of the measurement near the wall may be the cause. For the two-phase flow the computed profiles of liquid velocity agree well with the measured profiles at $X/D = 36$. This demonstrates the excellent capability of predicting the liquid velocity by the proposed model and present numerical method except near the wall. Furthermore, the predictions at the stations $X/D = 21$, 36 and 50 imply that the liquid velocity profiles are flattened near the wall as the flow goes downstream. The tendency of bubble movement towards the wall and the presence of the bubbles increase the diffusion and explain the above observation. The present work also obtains the gas phase velocity profiles at all locations and these plots indicate that the present approach can achieve reasonable predictions except near the wall. The results indicate that further improvements near the wall are needed. Figure 2 also reveals a near-uniform relative velocity between liquid and gas phases in the radial direction except near the pipe wall. The situations in which bubbles are sliding on the pipe wall implies that the gas velocity can be identified on the basis of the movement of the bubbles. Therefore the gas axial velocity near the wall is not reduced as the liquid phase velocity is. Thus the relative velocity near the wall becomes somewhat larger than the near-uniform value in the core region.

The development of a void profile is shown in more detail in Figures 3(a) and 3(b). The peak value of void fraction distribution is located at r/R around 0·9. More bubbles accumulate near the pipe wall as L/D increases. The peak value therefore increases as the fluid flows downstream. In contrast, the void fraction is decreasing in the core region. Similar results were observed in Serizawa's[20] experiment. However, Liu[21] reported an opposite trend showing the near-wall peaking of the void profile tends to be flattened in the downstream region. The conflict between the prediction and Liu's[21] observation may result from the assumptions of constant bubble size and no bubble coalescence or break-up. The bubble dynamics, which is not of primary concern and not considered in this study, is regarded as an important mechanism of the void fraction distribution by Zun *et al.*[22]

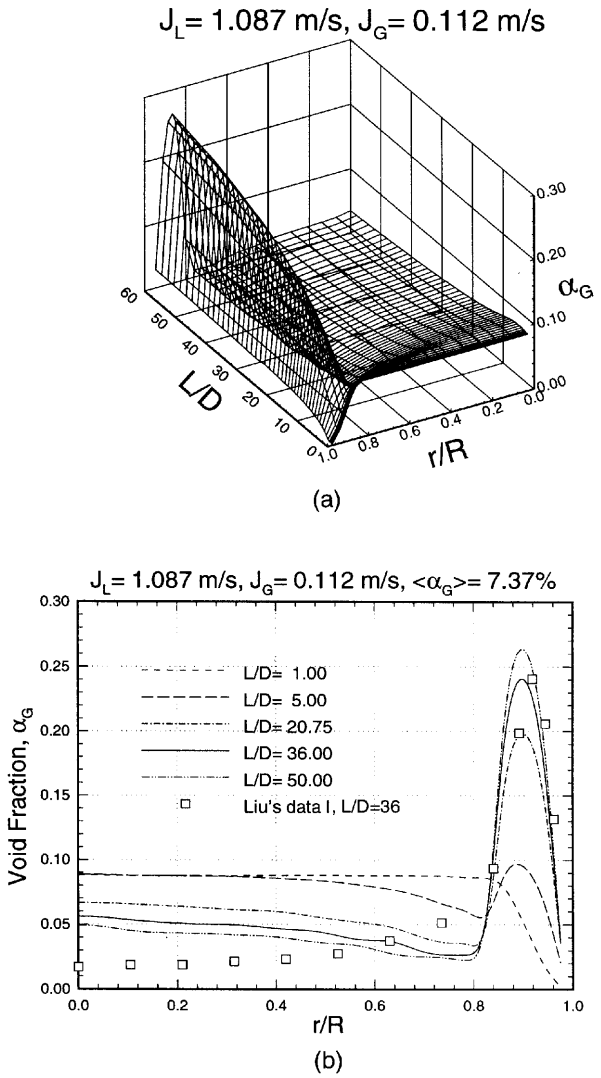

Figure 3. Development of void fraction distribution

The peak location of the void fraction result from two competitive forces, i.e. the lift force and wall force, acting on bubbles. Figure 4(a) presents a comparison of these two interfacial forces at several axial locations. The wall force exists near the pipe wall only and vanishes when $r/R < 0{\cdot}85$. The negative value of the wall force indicates that the gas bubble is pushed away from the pipe wall. In contrast, the lift force is positive, indicating that this force drives the gas bubble towards the channel wall. The lateral lift force is proportional to the velocity gradient (see equation (8)) and therefore is increased sharply and reaches a peak near the pipe wall. The balance of lateral force and wall force results in the peak location for a void profile as found in Figure 4(b). The sum of these two forces is zero at $r/R \approx 0{\cdot}9$, which is consistent with the peak location shown in Figure 3.

Figures 5 and 6 illustrate the comparison of model predictions of phasic velocity profiles, void fraction distribution and turbulent shear stress with experimental data for various superficial

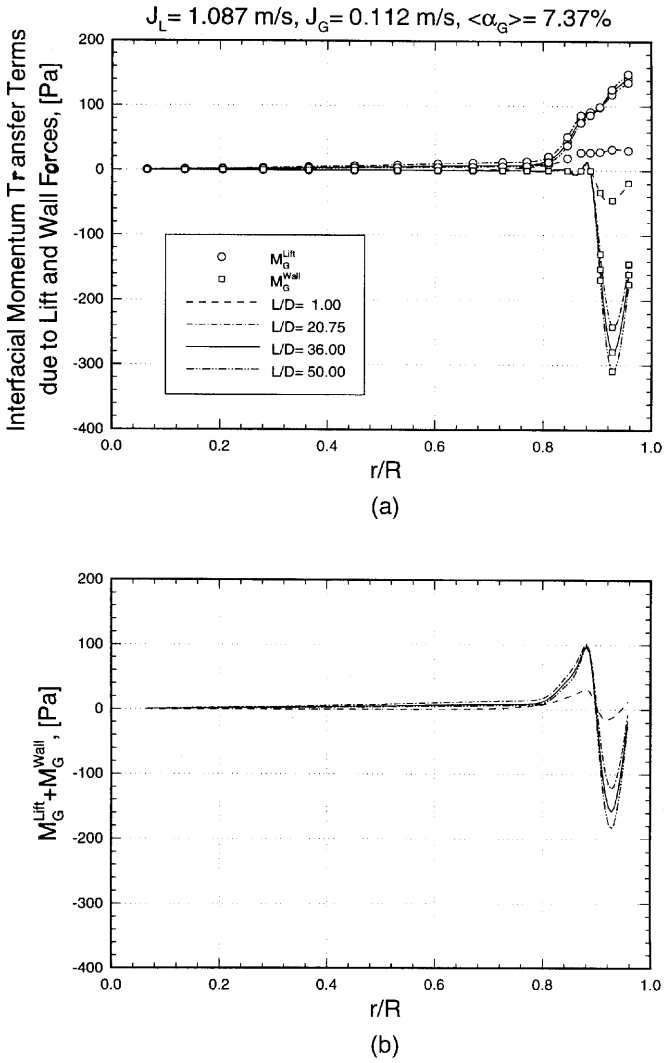

Figure 4. Distribution and comparison of interfacial momentum transfer due to lateral lift force and wall force in radial direction

velocities at a given superficial gas velocity and for various superficial gas velocities at a given superficial liquid velocity respectively. In general the predictions correlate well with Liu's[8] data, especially for those cases with a lower mean void fraction. The turbulent shear stresses shown in Figures 5(d) and 6(d) are somewhat overpredicted. However, the model predicts the same trends as the experiment.

Figure 7 shows an overall comparison of predictions with the experimental data of all 42 cases in Liu's[8] study. As shown in Figure 7(a), the present method accurately predicts the axial velocity distribution for the liquid phase. However, several points in Figure 7(a) are located outside the 20% error bands. These points are the two cases with a higher mean void fraction, i.e. 36·57% and 41·68%. These two cases are expected to be near the slug flow regime according to the model of Serizawa and Kataoka.[23] If these two conditions are excluded, more than 99% of the predictions are within the 20%

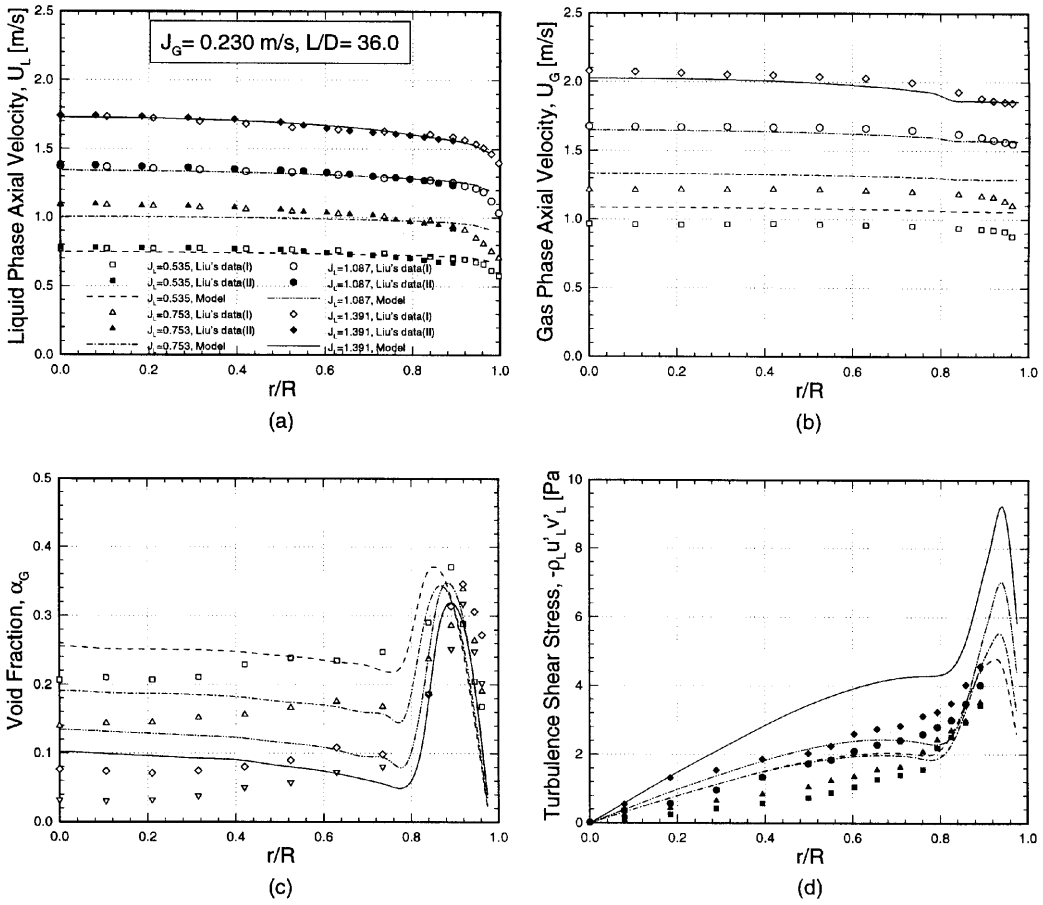

Figure 5. Comparison of predicted (a) axial velocity profile of liquid phase, (b) axial velocity profile of gas phase, (c) void fraction distribution and (d) turbulent shear stress $-\rho_L \overline{u'_L v'_L}$ with experimental data of Liu[8] at $L/D = 36{\cdot}0$ for $J_G = 0{\cdot}230$ m s^{-1} and $J_L = 0{\cdot}535$, $0{\cdot}753$, $1{\cdot}087$ and $1{\cdot}391$ m s^{-1}

error bands; in addition, more than 90% are within the 10% error bands. Further the correlations for the cases with larger superficial liquid velocities are better than those for the smaller ones both quantitatively and qualitatively. The overall comparison of predicted gas velocities with experimental data is presented in Figure 7(b). About 91% of the data points are predicted within the 20% error bands; in addition, almost all the data points are predicted within the 30% error bands. Figure 7(c) and 7(d) show the accuracy of the present model in predicting the void fraction α_G and turbulent shear stress $-\rho_L \overline{u'_L v'_L}$. About 55% of the data points of void fraction are predicted within the 30% error bands. Most of the points outside the error bands are located near the centreline of the pipe, where the model tends to overpredict the Reynolds stress values. As shown in Figure 7(d), the prediction of turbulent shear stress is less satisfactory, especially for those cases with a mean void fraction higher than 20%. However, acceptable predictions are obtained for the cases with $\langle \alpha_G \rangle$ less than 20%. This correlation shows the present model is more suitable for those cases with a small average void fraction ($< 20\%$); in addition, the model must be modified for the cases with a higher void fraction ($> 20\%$).

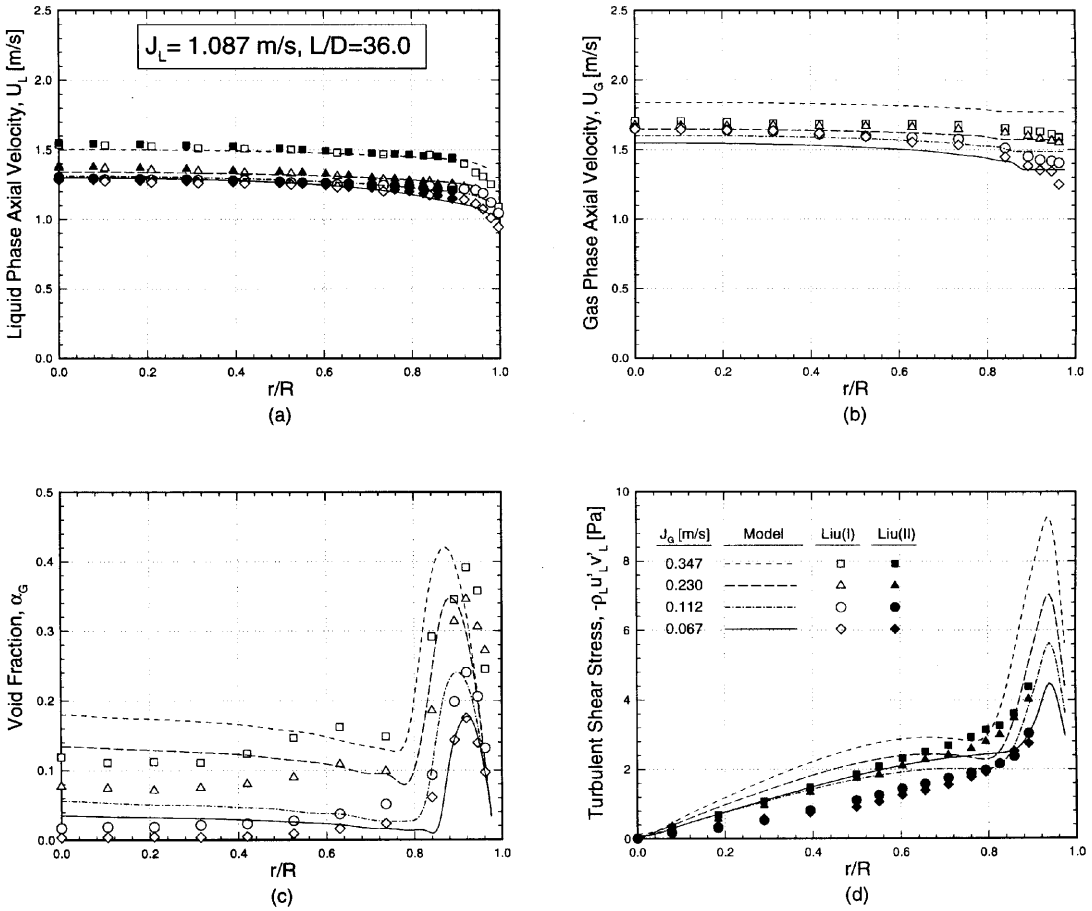

Figure 6. Comparison of predicted (a) axial velocity profile of liquid phase, (b) axial velocity profile of gas phase, (c) void fraction distribution and (d) turbulent shear stress $-\rho_L \overline{u'_L v'_L}$ with experimental data of Liu[8] at $L/D = 36{\cdot}0$ for $J_L = 1{\cdot}087$ m s^{-1} and $J_G = 0{\cdot}067$, $0{\cdot}112$, $0{\cdot}230$ and $0{\cdot}347$ m s^{-1}

CONCLUSIONS

A Eulerian formulation for the continuous (liquid) phase and a Lagrangian approach for the disperse (gas) phase have been proposed and employed in this study to investigate the multidimensional phase distribution for air–water two-phase bubbly flows. The developing two-phase flow characteristics, i.e. the velocities for both phases, void fraction distribution and liquid turbulent properties, can be obtained. The model predictions of various two-phase flow characteristics correlate well with the data of Liu[8] for low mean void fraction. The velocity fields for both phases are accurately predicted in most cases. The near-wall-peaking void fraction profiles are predicted for all cases with a sufficient correlation both in trend and magnitude. Also, the turbulent shear stress $-\rho_L \overline{u'_L v'_L}$ is overpredicted; however, the correct trend and magnitude can be obtained by the present model with a mean void fraction less than 20%.

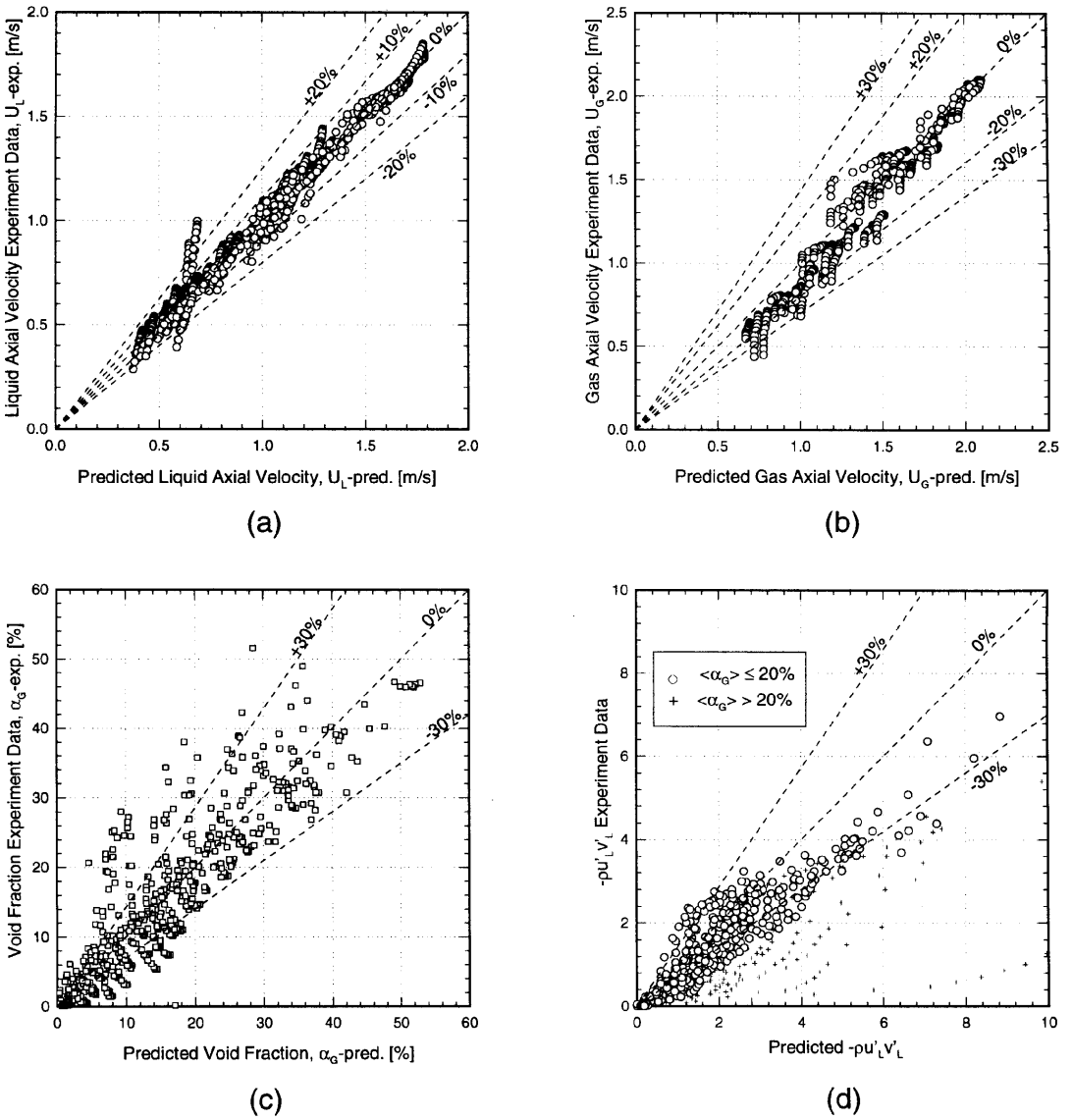

Figure 7. Comparison of predicted (a) axial velocity of liquid phase, (b) axial velocity of gas phase, (c) void fraction and (d) turbulent shear stress with experimental data of Liu[8] at $L/D = 36{\cdot}0$

REFERENCES

1. K. Rajagopal and L. Tao, *Mechanics of Mixtures*, World Scientific, Singapore, 1995.
2. S. P. Antal, R. T. Lahey Jr. and J. E> Flaherty, 'Analysis of phase distribution in fully developed laminar bubbly two-phase flow,' *Int. J. Multiphase Flow*, **17**, 635–652 (1991).
3. R. T. Lahey, Jr., 'Turbulence and phase distribution phenomena in two-phase flow', in *Transient Phenomena in Multiphase Flow*, Hemisphere, Washington, DC, 1987, pp. 139–177.
4. G. J. Lee and S. H. Chang, 'Physical modeling and finite element method for the analysis of lateral phase distribution phenomena,' *Proc. Int. Flows '91*, Tsukuba, September 1991.
5. O. Simonin and P. L. Viollet 'Numerical study on phase dispersion mechanisms in turbulent bubbly flows', *Proc. Int. Conf. on Mechanics of Two-Phase Flows*, Taipei, 1989, pp. 163–165.
6. C. T. Crowe, 'Review—numerical methods for dilute gas particle flows,' *ASEME J. Fluids Eng.*, **104**, 297–303 (1982).

7. F. Durst, D. Milojevic and B. Schoenung, 'Eulerian and Lagrangian predictions of particular two-phase flows: a numerical study,' *Appl. Math. Model.*, **8**, 101–115 (1984).
8. T. J. Liu, 'Experimental investigation of turbulence structure in two-phase bubbly flow', *Ph.D. Thesis*, Northwest University, 1989.
9. M. Ishii, *Thermal-Fluid Dynamics of Two-Phase Flow*, Eyrolles, Paris, 1975.
10. M. Ishii and N. Zuber, 'Drag coefficient and relative velocity in bubbly, droplet or particulate flows', *AIChE J.*, **25**, 843–855 (1979).
11. M. Ishii and K. Mishima, 'Two-fluid model hydrodynamic constitutive relation,' *Nucl. Eng. Des.*, **82**, 107–126 (1984).
12. D. A. Drew and R. T. Lahey Jr., 'The virtual mass and lift force on a sphere in rotating and straining inviscid flow,' *Int. J. Multiphase Flow*, **13**, 113–121 (1987).
13. S. K. Wang, S. J. Lee, O. c. Jones Jr and R. T. Lahey Jr., '3-D turbulence structure and phase distribution measurements in bubbly two-phase flows', **13**, 327–343 (1987).
14. R. Martinuzzi and A. Pollard, 'Comparative study of turbulence models in predicting turbulent pipe flow,' *AIAA J.*, **27**, 29–36 (1989).
15. B. E. Launder and D. B. Spalding, 'The numerical computation of turbulent flows,' *Comput. Methods Appl. Mech. Eng.*, **3**, 269–289 (1974).
16. Y. Sato, M. Sadatomi and K. Sekoguchi, 'Momentum and heat transfer in two-phase bubble flow,' *Int. J. Multiphase Flow*, **7**, 167–177 (1981).
17. de Bertodano *et al.* (1994).
18. C. M. Tchen, 'Mean value and correlation problems connected with the motion of a small particle suspended in a turbulent fluid', *Thesis*, University of Delft, 1947.
19. J. P. Van Doormaal and G. D. Raithby, 'Enhancements of the SIMPLE method for predicting incompressible fluid flows', *Numer. Heat Transfer*, **7**, 147–163 (1984).
20. A. Serizawa, 'Fluid-dynamic characteristics of two-phase flow', *Ph.D. Thesis*, Kyoto University, 1974.
21. T. J. Liu, 'Bubble size and entrance length effects on void development in a vertical channel.' *Int. J. Multiphase Flow, Int. J. Multiphase Flow*, **19**, 99–113 (1993).
22. I. Zun, I. Kljenak and S. Moze, 'Space–time evolution of the nonhomogeneous bubble distribution in upward flow,' *Int. J. Multiphase Flow*, **19**, 151–172 (1993).
23. A. Serizawa and I. Kataoka 'Phase distribution in two-phase flow', in *Transient Phenomena in Multiphase Flow*, Hemisphere, Wasington, DC, 1987, pp. 179–224.
24. C. T. Crowe, M. P. Sharma and D. E> Stock, 'The particle-source-in-cell method for gas droplet flow,' *ASME J. Fluids Eng.*, **99**, 325–332 (1977).

